Nanoscale

Accepted Manuscript

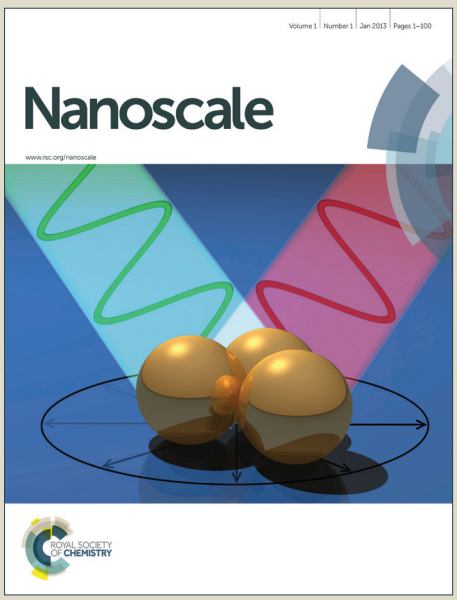

ROYAL SOCIETY OF CHEMISTRY

www.rsc.org/nanoscale

PEGylated Cu_3BiS_3 Hollow Nanospheres as a New Photothermal Agent for 980 nm-Laser-Driven Photothermochemotherapy and Contrast Agent for X-Ray Computed Tomography Imaging

Shu-Mei Zhou,[a] De-Kun Ma,*[a] Sheng-Hui Zhang,[b] Wei Wang,[b] Wei Chen,[a] Kang Yu*[b] and Shao-Ming Huang*[a]

Abstract

Developing multifunctional near-infrared (NIR) light-driven photothermal agents are highly demanded for efficient cancer therapy. Herein, PEGylated Cu_3BiS_3 hollow nanospheres (HNSs) with an average diameter of 80 nm were synthesized through a facile ethylene glycol-mediated solvothermal route. The obtained PEGylated Cu_3BiS_3 HNSs exhibited strong NIR optical absorption with a large molar extinction coefficient of 4.1×10^9 $cm^{-1} M^{-1}$ at 980 nm. Under the irradiation of a 980 nm laser with a safe power density of 0.72 W cm^{-2}, Cu_3BiS_3 HNSs produced significant photothermal heating with a photothermal transduction efficiency of 27.5%. The Cu_3BiS_3 HNSs also showed good antitumoral drug doxorubicin (DOX) loading capacity and pH- and NIR-responsive DOX release behaviors. At a low dosage of 10 μg/mL, HeLa cells could be efficiently killed through a synergistic effect of chemo- and photothermo-therapy respectively based on the DOX release and the photothermal effect of Cu_3BiS_3 HNSs. In addition, Cu_3BiS_3 HNSs displayed good X-ray computed tomography (CT) imaging capability. Furthermore, Cu_3BiS_3 HNSs could be used for efficient in vivo photothermochemotherapy and X-ray CT imaging of the mice bearing melanoma skin cancer. This multifunctional theranostic nanomaterial shows a potential promise for cancer therapy.

[a]*Nanomaterials and Chemistry Key Laboratory, Wenzhou University, Wenzhou, Zhejiang 325027, P. R. China*

[b]*Department of Hematology, The First Affiliated Hospital of Wenzhou Medical University, Wenzhou, Zhejiang 325027, P. R. China*

*Corresponding authors: dkma@wzu.edu.cn; yukang62@126.com; smhuang@wzu.edu.cn. Fax: +86-577-8837-3017; Tel: +86-577-8837-3031.

† Electronic supplementary information (ESI) available. See DOI:

1. Introduction

NIR light-driven photothermal effect has aroused much attention because of its great potential for a wide range of applications, such as drug delivery system and cancer therapy,[1, 2] remote thermal reaction,[3] welding of ruptured tissue,[4] controlled release of cells,[5] and so forth.[6] Among them, photothermal therapy (PTT) based on NIR light-responsive photothermal agents are especially attracting for cancer treatment owing to its high selectivity and minimal invasiveness. A variety of nanomaterials, such as gold nanostructures (nanorods, nanocages, nanostars, etc.),[7-9] carbon nanomaterials (e. g. nanotubes, graphene),[10-11] palladium nanosheets,[12] copper chalcogenide-based binary semiconductor nanocrystals,[13-15] MS_2 (M = Mo, W) nanosheets,[16, 17] and some organic nanoparticles have been explored as photothermal agents for PTT of cancer cells in vitro and in vivo.[18-20] Comparatively speaking, copper sulfides are ideal photothermal agents for PTT because of their low cost and cytotoxicity, facile synthesis and good photostability.[21] However, relatively low photothermal conversion efficiency of copper sulfides nanoparticles limited their applications.[22] Some methods such as the fabrication of superstructures,[14] adjustment of stoichiometric ratio of Cu to S,[23] and the utilization of surface plasmon resonance have been successfully used to improve photothermal conversion efficiency of copper sulfides.[24] Here, we present another strategy to enhance photothermal performance of copper sulfide, namely, introducing Bi element into copper sulfide and preparing ternary Cu_3BiS_3. The reasons that we select Cu_3BiS_3 are as follows. First, Cu_3BiS_3 has a much stronger optical absorption coefficient compared to other Cu-S based compounds because of the presence of localized Bi 6p states.[25] Secondly, Bi is an environmentally friendly element and has a long history of use as a therapeutic agent with low toxicity.[26] Furthermore, Bi possesses larger X-ray attenuation coefficient and leaves no residue in the organism, which is very suitable for X-ray CT imaging.[27] Very recently, Hu and Yang group have irrespectively reported that Cu_3BiS_3 nanoplates (excited at 915 nm laser)[28] and nanopartilces (excited at 808 nm laser)[29] could be used as potential photothermal agent and CT imaging contrast agent.

Current clinical therapy investigation has indicated that a combination of chemo- and thermotherapy can enhance therapeutic efficacy of cancer because hyperthermia can promote drug delivery into tumor and increase the drug toxicity.[30, 31] However, in this case the heat and drug do not take effect simultaneously in the same tumorgenic regions, which will cause side-effects and

unsatisfactory therapeutic efficiency. To overcome this problem, a synergistic system capable of co-delivery of chemotherapeutic agent and photothermal agent need to be developed. Recently, several nanocomposite systems such as silica/Au nanoshells,[32] silica/graphene nanosheets,[1] and PEG-graphene oxide/CuS have been used for photothermochemotherapy and showed apparently enhanced therapeutic efficacy.[33] However, the preparation of these composite materials often needs multistep processes and the stability of the products should also be further concerned. On the other hand, at present, X-ray CT is still considered as one of the most powerful diagnostic imaging techniques. Therefore it is highly desirable to obtain single-component nanomaterials with both photothermochemotherapy and imaging functions.

In this study, we present a new Cu_3BiS_3 HNSs PTT agent, which showed strong optical absorption with a large molar extinction coefficient of 4.1×10^9 cm^{-1} M^{-1} at 980 nm, for the ablation of human cervical cancer (HeLa) cell by the combination of photothermal therapy and chemotherapy. PEGylated Cu_3BiS_3 HNSs could be prepared through a facile ethylene glycol-mediated solvothermal route. The products exhibited good colloid stability and obvious amphiphilicity with the functionalization of PEG 2000. Large surface area and negative surface charge rendered Cu_3BiS_3 HNSs good loading capacity for positively charged DOX. DOX@PEGylated Cu_3BiS_3 HNSs system showed pH- and heat-responsive two-way drug release behaviors. In addition, it was found that Cu_3BiS_3 HNSs possessed good X-ray CT imaging function. The primary in vivo tests showed that PEGylated Cu_3BiS_3 HNSs had good effects for both photothermochemotherapy and X-ray CT imaging of the mice bearing melanoma skin cancer, suggesting that the nanomaterial could be used as future imaging-guided cancer therapy.

2. Experimental Section

2.1 Synthesis of PEGylated Cu_3BiS_3 HNSs. In a typical process, 0.45 mmol of $CuCl_2$ and 0.15 mmol of $Bi(NO_3)_3 \cdot 5H_2O$ were dissolved into 55 mL of ethylene glycol under thorough stirring. Then the solution was refluxed at 200 ^oC for 1 h. Subsequently, mixed solvents of PEG 2000 (4 mL) and ethylene glycol (5 mL) containing 0.6 mmol of L-cysteine were quickly injected into the above-mentioned solution. After that, the solution was put into a Teflon-lined stainless-steel autoclave with 150 mL of capacity and heated at 200 ^oC for 1 h. After it was cooled to room temperature, the resulting black precipitate was separated by centrifugation and washed with

deionized water and absolute ethanol for several times. Then the products were dried at 60 ^{o}C for 4 h under vacuum for further characterizations.

2.2 Characterization. Transmission electron microscopy (TEM) image, high-resolution transmission electron microscopy (HRTEM) image, scanning transmission electron microscopy (STEM) image, energy dispersive X-ray spectroscopy (EDS), and elemental mapping were performed on a JEM-2100F HRTEM, using an accelerating voltage of 200 kV. The crystallographic structure and phase purity of the products were examined by powder X-ray diffraction (XRD) patterns obtained on a Bruker D8 Advanced X-ray diffractometer, using Cu-Ka radiation (λ = 0.15418 nm) at a scanning rate of 8^{o} min^{-1} in the 2θ range of 10-70^{o}. X-ray photoelectron spectroscopy (XPS) measurement was carried out with a Thermo ESCALAB 250 X-ray photoelectron spectrometer with an excitation source of Al Kα radiation (λ = 1253.6 eV). Fourier-transform infrared (FT-IR) spectrum was recorded on a Bruker EQUINOX 55 FTIR spectrometer in the range of 4000 to 400 cm^{-1}. The thermogravimetric (TG) analysis was carried out on a Diamond TG-DTA thermal analysis instrument (Perkin Elmer) under nitrogen. UV-vis absorption spectra were recorded on a UV2501PC (Shimadzu). The zeta (ζ) potential measurement was carried out on a Zetasizer nano ZS90 (Malvern). The Brunauer-Emmett-Teller (BET) surface area was measured with an ASAP2020 specific surface area analyzer.

2.3 Measurement of Photothermal Conversion Efficiency. In order to measure the photothermal conversion efficiency of the synthesized PEGylated Cu_3BiS_3 HNSs, a continuous wave 980 nm laser with tunable power was used to irradiate the solution containing the nanoparticles at a concentration of 50 μg/mL. The output power was calibrated through an optical power meter (Newport model 1918-C, CA, U.S.A.) and fixed at a safe power density of 0.72 W cm^{-2}. The temperature was recorded by a thermocouple thermometer (DT-8891E Shenzhen Everbest Machinery Industry Co., Ltd., China) with an accuracy of ±0.1 °C every 20 s.

2.4 Loading capacity and photothermal-driven release of DOX. To load DOX, 10 mg of the above prepared PEGylated Cu_3BiS_3 HNSs were dispersed in DOX aqueous (20 mL, 0.1 mg/mL) and stirred in the dark at room temperature for 48 h to ensure an adsorption–desorption equilibrium between the nanoparticles and DOX. After that, the solution was centrifuged and the supernatants were quantitatively analyzed by Shimadzu UV2501PC spectrophotometry at 480 nm. The loading capacity could be expressed by eq 1

Loading capacity (mg/mg) = mass of loaded DOX(mg)/mass of Cu_3BiS_3 HNSs (mg)

The release of DOX was carried out at ambient temperature. 2 mg of DOX@PEGylated Cu_3BiS_3 HNSs were dispersed in 2 mL of phosphate buffered saline (PBS) at certain pH values. The solution was standing in dark for 1 h. Then a 980 nm laser with an output power density of 0.72 Wcm^{-2} was used to irradiate the solution for 5 min. Such operations were repeated for five times. At given time intervals, the solution containing nanoparticles were centrifuged and the supernatants withdrawn for analysis of DOX before and after NIR laser irradiation. The concentration of DOX in the supernatant was determined by spectrophotometry.

2.5 Cell viability assay. HeLa cells were used to evaluate the cellular cytotoxicity of the sample. They were cultured using established procedures. The HeLa cells were seeded in 96-cell plates at a density of 4×10^3 and cultured in a humidified incubator at 37 ^oC, 5% of CO_2 for 24 h. After that, the culture medium was removed and replaced with Dulbecco's Modified Eagle's Medium (DMEM) supplemented with fetal bovine serum containing PEGylated Cu_3BiS_3 HNSs with different doses. The cells were incubated for another 24 h. Then 20 μL of 3-(4, 5-dimethylthiazol-2-yl)-2, 5-diphenyltetrazolium bromide (MTT) solution (5 mg/mL) was added to each well. The 96-well cell plates were further incubated in a 5% of CO_2 humidified incubator at 37 ^oC for 4 h, followed by removing the culture medium with MTT. Then 200 μL of dimethysulfoxide was added into each well. The resulting mixture was shaken for *ca*. 10 min at room temperature. The optical density of the mixture was measured at 490 and 630 nm by a double-wavelength microplate reader (Tecan). The cell viability was calculated by assuming 100% viability in the control group without any PEGylated Cu_3BiS_3 HNSs.

2.6 In Vitro Photothermochemotherapy. To study combined chemo- and photothermo-therapy effect of PEGylated Cu_3BiS_3 HNSs, HeLa cells were seeded in 96-well plates with a density of 5×10^4 for 12 h and set six groups (control, laser, DOX, Cu_3BiS_3 HNSs + DOX, Cu_3BiS_3 HNSs + laser, Cu_3BiS_3 HNSs + DOX + laser). Specifically, when cells had grown to 90% in plates, the first group had no treatment. The second one was only irradiated with 980 nm laser. The third one was treated with different concentrations of DOX (0.1, 0.5, 1, 5 and 10 μg/mL). The fourth one was incubated with different concentrations of DOX@Cu_3BiS_3 HNSs (0.1, 0.5, 1, 5 and 10 μg/mL) for 24 h. The fifth and sixth ones were incubated with different concentrations of Cu_3BiS_3 HNSs and DOX@Cu_3BiS_3 HNSs (0.1, 0.5, 1, 5 and 10 μg/mL) for 24 h, at the same time, irradiated with

laser, respectively. The cell viability was measured using the above-mentioned MTT method. Every group test was repeated for six times. To identify the cell viability, the dead cells were stained with Trypan Blue.

2.7 In vitro CT imaging. PEGylated Cu_3BiS_3 HNSs were dispersed in PBS with different concentrations in the range from 0.006 to 0.096 M. CT images were recorded on a microCT (eXplore Locus) system. Imaging parameters were set as follows: thickness, 0.9 mm; voltage, 120 KVp; current, 300 mA; gantry rotation time, 0.5 s; table speed, 158.9 mm/s.

2.8 In vivo photothermochemotherapy of skin cancer. Animal procedures have complied with the guidelines of the Institutional Animal Care and Use Committee. For in vivo tests, Balb/c mice were inoculated subcutaneously with 2×10^6 B16 cells, a mouse melanoma cell line, at backside. The mice were used for treatment when the tumor volume reached ca. 80 mm^3. Then 8 mice were randomly divided into 4 groups (each tests were carried out twice), and PBS solution (Group I), PEGylated Cu_3BiS_3 HNSs + DOX (Group II, 10 mg/mL), PEGylated Cu_3BiS_3 HNSs + laser (Group III, 10 mg/mL) and EGylated Cu_3BiS_3 HNSs + DOX + laser (Group IV, 10 mg/mL) were locally injected into the tumors intratumorally. Then the 980 nm continuous-wave NIR laser was used to irradiate tumors in group III and IV at a power density of 0.72 Wcm^{-2} for 10 min. After 48 h, the mice were killed. The tumor tissues were peeled from mice and fixed in 4% formaldehyde solution (pH = 7.0). The tissues were processed with paraffin embedding routinely, and 3.5 μm-thick sections were cut and placed on glass slides, followed by staining with hematoxylin and eosin. Finally, the pathological sections were determined at × 100 magnification using common fluorescence microscope.

2.9 In vivo CT imaging. Two Balb/c mice bearing melanoma tumors were anesthetized with trichloroacetaldehyde hydrate (10%, 100 μL). One mouse was intratumorally injected into Cu_3BiS_3 HNSs (100 μL, 50 mg/mL), while the other was not done (contrast group). In vivo CT scanning was performed after injection of the Cu_3BiS_3 HNSs at the time points of 2 h post-injection. All CT scans were performed using the microCT system with the parameters similar to those for in vitro experiments.

3. Results and Discussion

Typical TEM image showed that the products were hollow nanospheres with an average

diameter of 80 nm (Fig. 1a). These hollow nanospheres were fabricated by smaller nanoparticles, which can be clearly revealed by HRTEM images (Fig. 1b). The lattice fringe with a spacing of about 0.31 nm is in good agreement with the interplanar separation of (220) planes of orthorhombic-phase Cu_3BiS_3. Fig. 1c-f represents STEM image recorded on an individual nanosphere and its corresponding elemental mapping. It can be seen that Cu, Bi, and S elements are distributed uniformly across the whole nanosphere. The EDS of the products analysis showed that the ratio of Cu to Bi and S was *ca*. 3: 0.98: 2.97, which is close to stiochiometrci proportion of Cu_3BiS_3 (see ESI, Fig. S1)

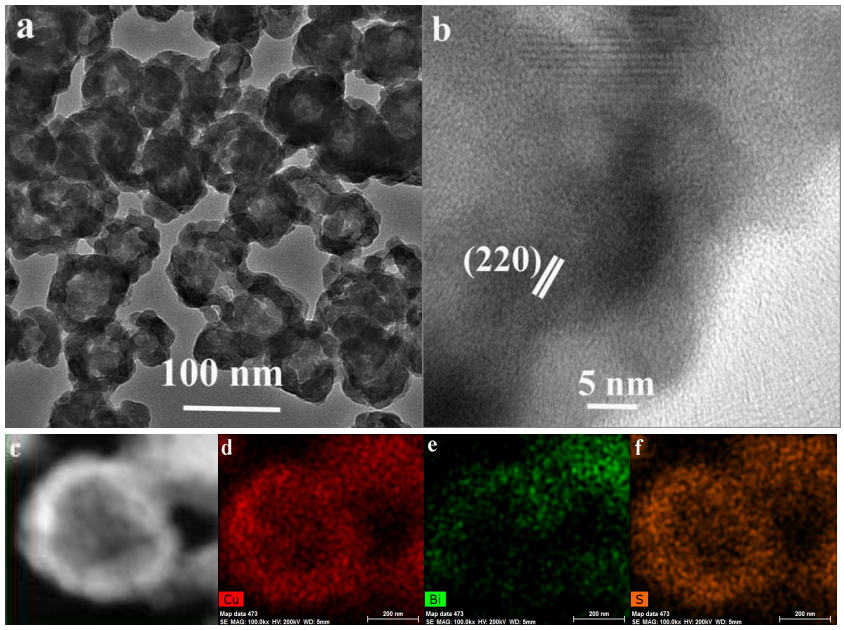

Fig. 1 (a) TEM image of the synthesized Cu_3BiS_3. (b) HRTEM image recorded on the rim of a single hollow nanosphere. (c) STEM image of an individual Cu_3BiS_3 hollow nanosphere. (d-f) Elemental mapping of the Cu_3BiS_3 hollow nanosphere.

XRD was used to study the crystallinity and phase structure of the as-synthesized hollow nanospheres. As can be seen from the XRD pattern in Fig. 2, the products show high crystallinity. All diffraction peaks could be indexed to pure orthorhombic-phase Cu_3BiS_3 (JCPDS No. 43-1479). No diffraction peaks from impurities and/or other phases could be detected, indicating the high purity of the final products. To understand the chemical states of Cu, Bi and S elements in the final products, XPS analyses were carried out (Fig. S2). Wide-scan XPS survey spectrum indicated that the products were composed of Cu, Bi, S, C and O elements. Cu, Bi, and S elements correspond to Cu_3BiS_3. C and O elements mainly come from PEG 2000. The binding energies of Bi 4f7/2 and Bi

4f5/2, Cu 2p3/2 and Cu 2p1/2, and S 2p obtained from corresponding high resolution XPS spectra were located at 158.2 and 163.5 eV, 930.8 and 950.7 eV, and 162.4 eV, respectively, which are consistent with previous report on Cu_3BiS_3.[34] Therefore the valence states of Bi, Cu, and S in Cu_3BiS_3 HNSs are +3, +1, and -2 valences, respectively. It should be pointed out here that no Cu^{2+} ions and Cu^0 were detected in the final products, although Cu^{2+} ions were selected as raw materials.

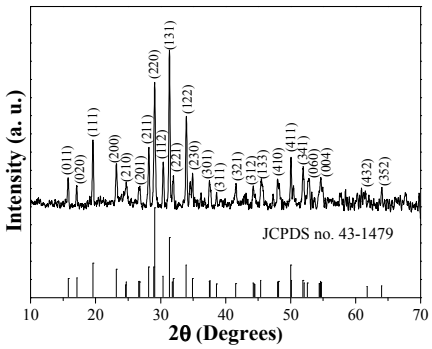

Fig. 2 XRD pattern of the products.

The surface PEGylation of nanoparticles has been widely used to improve their biocompatibility, render them resistant against protein adsorption, and stabilize them against agglomeration in biological environments.[35-37] Typical, a PEG chain with molecular weight of 2000 or greater is required to achieve stealth characteristics and avoid being caught by the phagocytic cells.[38] FT-IR absorption spectrum confirmed successful coating of PEG 2000 molecules on the surfaces of Cu_3BiS_3 HNSs, with characteristic peaks of PEG appearing at 3447 cm^{-1}, 2890 cm^{-1}, 1118 and 1439 cm^{-1} corresponding to O-H, C-H, and C-O stretching and C-H bending vibrations, respectively (Fig. S3). The content of PEG 2000 in the products was estimated to be *ca*. 5 wt% through TG loss curve analysis (Fig. S4). After PEGylation, Cu_3BiS_3 HNSs could be easily dispersed into water, ethanol and toluene, and displayed obvious amphiphilicity (Fig. S5a). Especially, the Cu_3BiS_3 colloid aqueous solution could keep good stability and no obvious precipitation was observed after 30 minutes' or more long standing (Fig. S5b).

The UV-vis absorption spectrum of PEGylated Cu_3BiS_3 HNSs was shown in Fig. 3. The sample exhibited strong absorption in NIR region with monotonically rising absorbance at wavelength above 750 nm. With increasing concentration of Cu_3BiS_3 HNSs, the corresponding absorbance linearly enhanced, which also confirmed good dispersity of Cu_3BiS_3 HNSs in water without any

macroscopic aggregates (Fig. S6). The molar extinction coefficient of Cu_3BiS_3 HNSs at 980 nm could be calculated by eq 2[39]

$$\varepsilon = (A\frac{\pi}{6}d^3\rho N_A)/(LC_{wt})$$

where A, d, ρ, N_A, L and C_{wt} are the absorbance at 980 nm, average diameter of nanospheres, density of nanospheres, Avogadro's constant, pathlength through the sample and weight concentration of the nanospheres, respectively. The absorbance value is 0.21 at 980 nm when the concentration of the solution is 50 μg/mL (Fig. S6a). L is equal to 1 cm. The density ρ for bulk Cu_3BiS_3 is about 6.19 g/cm^3. The density of Cu_3BiS_3 HNSs was approximately replaced by bulk one. Therefore the so obtained molar extinction coefficient is *ca*. 4.1 × 10^9 cm^{-1} M^{-1} at 980 nm, which is significantly larger than some other binary Cu-based compounds, such as CuS (3 × 10^7 cm^{-1} M^{-1}),[40] $Cu_{2-x}S$ (1 × 10^8 cm^{-1} M^{-1}),[41] and $Cu_{2-x}Se$ (7.7 × 10^7 cm^{-1} M^{-1}).[15]

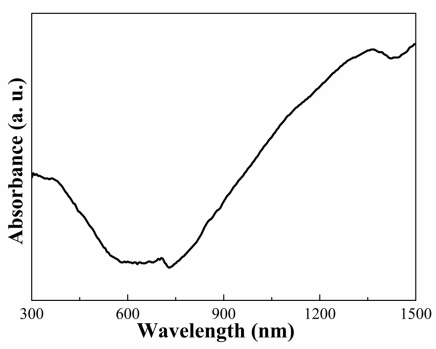

Fig. 3 UV-vis absorption spectrum of Cu_3BiS_3 HNSs.

The strong absorption at 980 nm makes PEGylated Cu_3BiS_3 HNSs highly promising for 980 nm laser-responsive photothermal agent. To investigate photothermal performance, the heating curves of the aqueous dispersion of Cu_3BiS_3 HNSs with different concentrations (1, 5, 25, 50, and 100 μg/mL) were measured under the irradiation of 980 nm laser (0.72 W cm^{-2}), and pure water was used as a negative control. As shown in Fig. 4a, the temperature of the solution raised rapidly with increasing irradiation time or the concentration of Cu_3BiS_3 HNSs. After irradiation of 600s, the final temperature of Cu_3BiS_3 HNSs solution was increased by 19.1 ^{o}C at a concentration of 100 μg/mL, while the temperature of pure water increased by only 9.3 ^{o}C (Fig. 4b). To further obtain photothermal conversion efficiency, the temperature change of the solution (50 μg/mL) was recorded as a function of time under continuous irradiation of the 980 nm laser (0.72 W cm^{-2}) until the solution reached a steady-state temperature (Fig. 4c, d). The photothermal conversion

efficiency was calculated through eq 3 [42]

$$\eta = \frac{hS\left(T_{Max} - T_{Surr}\right) - Q_{Dis}}{I\left(1 - 10^{-A_{980}}\right)}$$

where h, S, T_{Max}, T_{Surr}, Q_{Dis}, I, and A represent heat transfer coefficient, the surface area of the container, the equilibrium temperature, ambient temperature of the surroundings, the heat dissipation from the light absorbed by the quartz sample cell, the laser power, and the absorbance of the Cu_3BiS_3 HNSs at 980 nm, respectively. The value of hS is obtained through eq 4

$$hS = \frac{m_w C_w}{\tau_s}$$

where τ_s is the sample system time constant, m_w and C_w are the mass (1 g) and heat capacity (4.2 J/g) of water used as the solvent, respectively. The Q_{Dis} was measured independently using a quartz cuvette cell containing pure water without the Cu_3BiS_3 HNSs. T_{Max}, T_{Surr}, and τ_s were obtained from Fig. 4c and 4d to be 43.8 ^{o}C, 25 ^{o}C, and 284 s, respectively. The value of Q_{Dis} was *ca*. 0.203 W. Therefore the photothermal conversion efficiency of Cu_3BiS_3 HNSs at 980 nm was calculated to be 27.5%, which is higher than other Cu-based binary compounds, such as $Cu_{2-x}S$ (16%, 980 nm laser),[43] Cu_9S_5 (25.7%, 980 nm laser),[39] and $Cu_{2-x}Se$ nanocrystals (22%, 800 nm laser).[15] In order to further test Cu_3BiS_3 HNSs have better photothermal performance than other binary Cu-based semiconductors, Cu_9S_5 and CuS micro- and nanocrystals were prepared under similar synthetic conditions (see ESI, Fig. S7-10). As can be seen from temperature profiles of Cu_3BiS_3 HNSs, Cu_9S_5 and CuS flower-like superstructures aqueous solution performed at the same conditions (100 μg/mL, irradiated by a 980 nm laser), Cu_3BiS_3 HNSs showed the best photothermal heating performance (Fig. S11). In addition, the Cu_3BiS_3 HNSs could still keep good photothermal stability after five times cycle tests (laser on and off, Fig. S12)

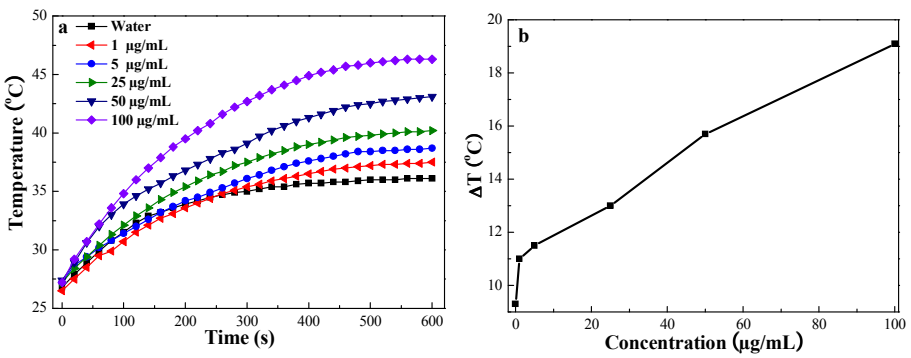

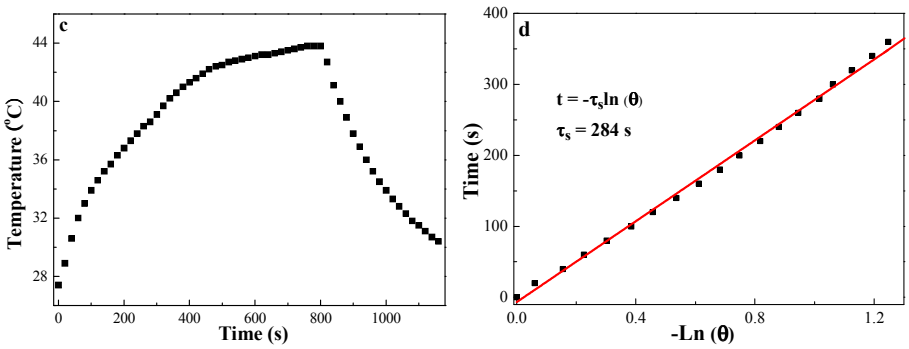

Fig. 4 (a) Temperature profiles of pure water and Cu_3BiS_3 HNSs aqueous solution at different concentrations. (b) Plot of temperature change (ΔT) over a period of 600 s versus the concentration of Cu_3BiS_3 HNSs. (c) The photothermal response of the Cu_3BiS_3 HNSs aqueous solution (50 μg/mL) under irradiation of an NIR laser (980 nm, 0.72 W cm^{-2}) for 600 s and then the laser was shut off. (d) Plot of cooling time versus –ln(θ) obtained from the cooling stage as shown in (c).

The synthesized Cu_3BiS_3 nanospheres have hollow interior structures, suggesting that they will have a large specific surface area. The N_2 adsorption-desorption isotherm and pore-size distribution curve analyses indicated that the Cu_3BiS_3 HNSs had a BET surface area of 10.2 m^2 g^{-1} and pore volume of 0.07 cm^3 g^{-1}(Fig. S13). The ζ potential measurement revealed that Cu_3BiS_3 HNSs had negative surface charge (-17.6 mV) due to the coating of PEG 2000 molecules (Fig. S14). Hollow interior structure, large surface area, and negative surface charge make Cu_3BiS_3 HNSs suitable for loading anticancer drug DOX with positive charge. As shown in Fig. 5, 60.8% of DOX molecules could be loaded on the surfaces of PEGylated Cu_3BiS_3 HNSs after adsorption equilibrium. The loading capacity of PEGylated Cu_3BiS_3 HNSs could reach 122 μg/mg, comparable to Cu_9S_5@$mSiO_2$-PEG core-shell nanocomposites with a large BET surface area of 221 m^2 g^{-1} (160 μg/mg).[44]

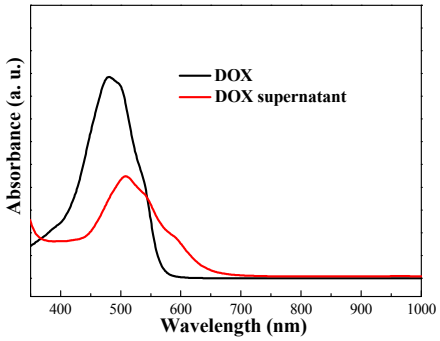

Fig. 5 UV-vis absorption spectra of initial DOX and the DOX supernatant after adsorption equilibrium.

To an efficient drug delivery system, it should also possess sustained-release ability. In order to evaluate this performance of DOX@PEGylated Cu_3BiS_3 HNSs, we measured DOX release behaviors at different pH values at 37 ^oC. As shown in Fig. 6a, DOX@PEGylated Cu_3BiS_3 HNSs system displayed pH-dependent DOX release behaves. The DOX release rate was much larger at pH = 5 than at pH = 7. Only 5.9% and 14.9% of the total bound DOX was released from DOX@PEGylated Cu_3BiS_3 HNSs within 10 h under neutral and acid conditions, respectively, which showed the sustained drug-release behavior of the present system. The enhancement of DOX release capability at lower pH could be ascribed to more of the $-NH_2$ groups on DOX are protonated with the decrease of pH, which increases the hydrophilicity and solubility of DOX and thus leads to the release of more of the incorporated DOX. The above mentioned DOX release behavior benefits cancer therapy because the microenvironments of extracellular tissues of tumors and intracellular lysosomes and endosomes are acidic, and this acidity can facilitate active drug release from Cu_3BiS_3 HNSs-based delivery vehicles.[45]

A 980 nm laser could be further used to control release of DOX from DOX@PEGylated Cu_3BiS_3 HNSs system. As shown in Fig. 6b, the irradiation of 980 nm laser could enhance the release of DOX, especially in the case of lower pH value. After five-minute irradiation (begun at 1 h, pH = 5, output power density of 0.72 W cm^{-2}), the cumulative release increased from 4.5% to 10.7%. The release of DOX slowed when the NIR laser was switched off over the next run of 1 h. Similar results were observed when the laser treatment protocol was repeated beginning at 2 h. However, the release rate of DOX gradually reduced with increasing cycle times. The results demonstrated that photothermal heating could enhance and control the release of DOX from

DOX@ PEGylated Cu_3BiS_3 HNSs system.

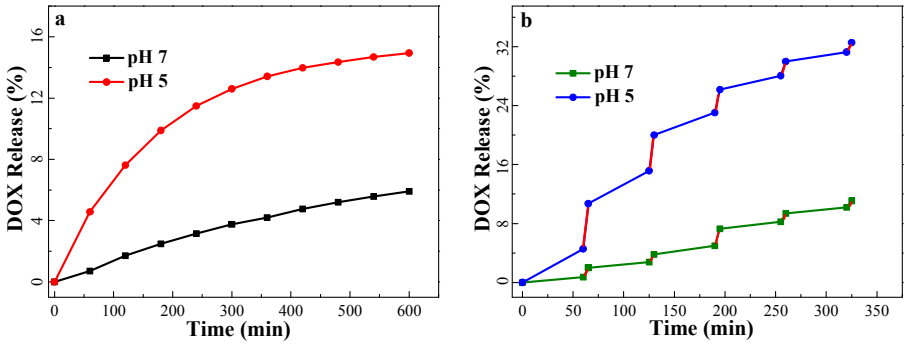

Fig. 6 (a) Effect of pH on DOX release from DOX@ PEGylated Cu_3BiS_3 HNSs system. (b) 980 nm laser-triggered release of DOX from DOX@ PEGylated Cu_3BiS_3 HNSs system at different pH conditions. Red lines represent the stage of laser irradiation.

For further biomedical applications, the cytotoxicity of these PEGylated Cu_3BiS_3 HNSs should be evaluated. HeLa cell was chosen as tumor cell model and the cytotoxicity of PEGylated Cu_3BiS_3 HNSs at different concentrations was assayed by standard MTT method. Negligible cytotoxicity was observed even when the incubation concentration of PEGylated Cu_3BiS_3 HNSs reached 600 μg/mL (Fig. 7).

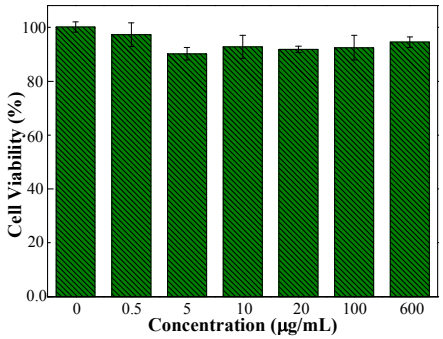

Fig. 7 Cytotoxicity evaluation of PEGylated Cu_3BiS_3 HNSs at different concentrations.

Substantial photothermal heating, good release function of DOX induced by 980 nm laser, and low cytotoxicity make DOX@PEGylated Cu_3BiS_3 HNSs promising application in combined photothermo- and chemo-therapy. As shown in Fig. 8a, the 980 nm laser irradiation alone caused no cell damage for a control group in the absence of PEGylated Cu_3BiS_3 HNSs. However, cell inhibitation rates obviously ascended with increasing concentration of Cu_3BiS_3 HNSs under irradiation of 980 nm laser with output power density of 0.72 W cm^{-2} for 5 min (Fig. 8b). At a very

lower dosage of 10 μg/mL, almost 100% of the HeLa cells were efficiently killed. Although DOX and DOX@Cu_3BiS_3 HNSs treatments could also kill cancer cells, only 52.6% and 35.8% of cells were broken at a dosage of 10 μg/mL, respectively. Clearly, the combination of photothermal therapy and chemotherapy exhibited the best effects because photothermal heating not only caused cell death itself but also triggered the release of DOX for enhanced chemotherapy. As shown in Fig. 8a, at each concentration, photothermochemotherapy exhibited the highest cytotoxicity compared to single chemotherapy or photothermal therapy, which really reflected the synergistic effect of photothermal therapy and chemotherapy of the Cu_3BiS_3 HNSs system.

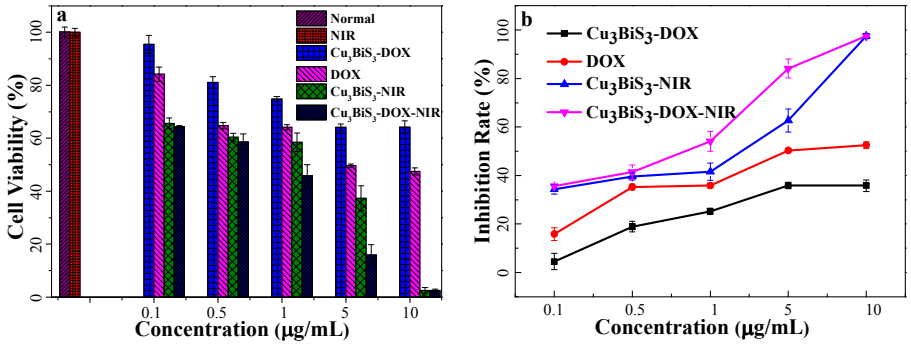

Fig. 8 (a) Cell viability under different treatment conditions. (b) The corresponding inhibitation rate of cell after treatment.

In order to show visually the effect of photothermochemotherapy over DOX@Cu_3BiS_3 HNSs, micrographs of HeLa cells after treatment stained with Trypan Blue were taken. As shown in Fig. 9b, no dead cells were found only under the irradiation of 980 nm laser. However, in the presence of 10 μg/mL of DOX@Cu_3BiS_3 HNSs, HeLa cells were almost killed completely (Fig. 9d). The results are consistent with above MTT assays.

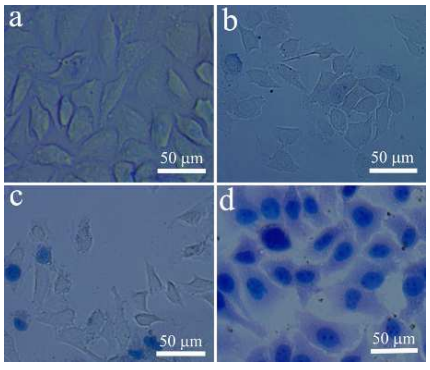

Fig. 9 Micrographs of HeLa cells treated under different conditions: (a) without any treatment, (b)

only irradiation under 980 nm laser, (c) 0.1 μg/mL of DOX@Cu_3BiS_3 HNSs plus laser, and (d) 10 μg/mL of DOX@Cu_3BiS_3 HNSs plus laser. Dead cells were stained with Trypan Blue.

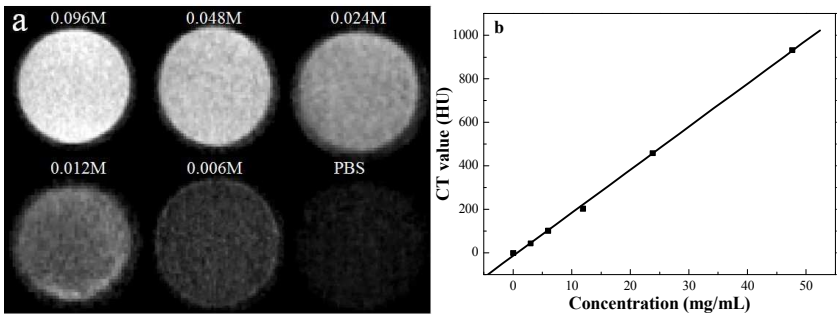

Fig. 10 (a) In vitro CT images of PEGylated Cu_3BiS_3 HNSs with different concentrations. (b) CT value (HU) of PEGylated Cu_3BiS_3 HNSs as function of the concentration.

Bi-based nanomaterials such as Bi_2S_3 and Bi_2Se_3 have been proved to be ideal CT contrast agents because Bi possesses large X-ray attenuation coefficient, low toxicity, and leave no residue in the organism.[27, 46] To evaluate the CT contrast performance of the synthesized Cu_3BiS_3 HNSs, in vitro CT imaging test was carried out. As shown in Fig. 10a, CT signal intensity gradually enhanced with increasing Cu_3BiS_3 concentrations. Correspondingly, the Hounsfield units (HU) values ascended linearly with the increase of concentrations of Cu_3BiS_3 HNSs (Fig. 10b). The slope of the HU value for Cu_3BiS_3 HNSs was about 19.81, and it is higher than that of iopromide (16.38).[47] Therefore Cu_3BiS_3 HNSs could provide an equivalent contrast at a lower dose compared to the clinical iodine agent.

Furthermore, in vivo photothermochemotherapy and X-ray CT imaging of the mice bearing melanoma skin cancer over PEGylated Cu_3BiS_3 HNSs were carried out. The tumor-bearing mice were divided into 4 groups: PBS solution (Group I), PEGylated Cu_3BiS_3 HNSs + DOX (Group II), PEGylated Cu_3BiS_3 HNSs + laser (Group III) and PEGylated Cu_3BiS_3 HNSs + DOX + laser (Group IV). After different treatments, histological examination was performed (Fig. 11). In marked contrast, large numbers of necrotic cells were observed after the treatment of PEGylated Cu_3BiS_3 HNSs + DOX + laser for 10 min (Fig. 11d). The results are in agreement with in vitro photothermochemotherapy of HeLa cells. On the other hand, in vivo CT imaging was done on the mice bearing melanoma skin cancer treated with or without PEGylated Cu_3BiS_3 HNSs. As a result,

the tumor containing Cu_3BiS_3 HNSs displayed a brighter contrast (marked with empty circle) than other soft tissues and the tumor without any treatment (Fig. S15). The above features suggest that Cu_3BiS_3 HNSs are good CT contrast agents and promising for application in imaging-guided photothermochemotherapy.

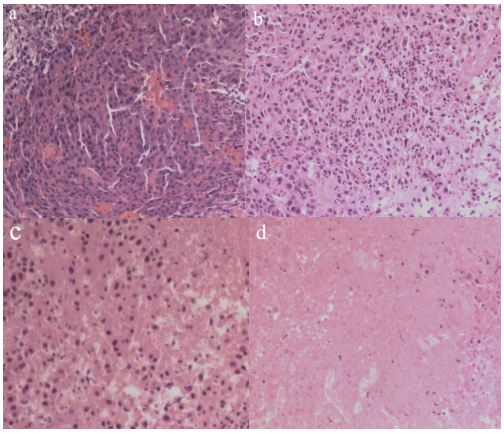

Fig. 11 Hematoxylin and eosin stained histological images of ex vivo tumor sections treated under different conditions: (a) PBS solution, (b) PEGylated Cu_3BiS_3 HNSs + DOX, (c) PEGylated Cu_3BiS_3 HNSs + laser, and (d) PEGylated Cu_3BiS_3 HNSs + DOX + laser.

4. Conclusions

In summary, we have synthesized PEGylated Cu_3BiS_3 HNSs as a highly efficient photothermal agent through a facile solvothermal route on a large scale. The resultant Cu_3BiS_3 HNSs showed negative surfaces charge because of the coating of PEG 2000. As a result, the products could keep good colloid stability, display obvious amphiphilicity, and efficiently load positively charged DOX molecules. The DOX@PEGylated Cu_3BiS_3 HNSs system showed pH-responsive release behavior of DOX. Under the irradiation of 980 nm laser, the release capability of DOX could be further enhanced, especially in the case of lower pH value. Importantly, a synergistic effect in killing cancer cells both in vitro and in vivo was found by the combined chemo- and photothermo-therapy. Furthermore, the synthesized Cu_3BiS_3 HNSs showed promising application in CT imaging and can be further developed as a CT imaging-guided photothermochemotherapy platform in the future.

Acknowledgments. This work was financially supported by NSFC (51372173, 51002107, and

21173159), NSFC for Distinguished Young Scholars (51025207), Research Climb Plan of ZJED (pd2013383), and Opening Project of State Key Laboratory of High Performance Ceramics and Superfine Microstructure (SKL201409SIC).

Reference and Notes

1. Y. Wang, K. Y. Wang, J. F. Zhao, X. G. Liu, J. Bu, X. Y. Yan and R. Q. Huang, *J. Am. Chem. Soc*., 2013, **135**, 4799.
2. J. O. You, P. Guo and D. T. Auguste, *Angew. Chem. Int. Ed*., 2013, **52**, 4141.
3. S. J. Pastine, D. Okawa, A. Zettl and J. M. J. Frechet, *J. Am. Chem. Soc*., 2009, **131**, 13586.
4. H. C. Huang, C. R. Walker, A. Nanda and K. Rege, *ACS Nano*, 2013, **7**, 2988.
5. W. Li, J. S. Wang, J. S. Ren and X. G. Qu, *Angew. Chem. Int. Ed*., 2013, **52**, 6726.
6. C. H. Zhu, Y. Lu, J. Peng, J. F. Chen and S. H. Yu, *Adv. Funct. Mater*., 2012, **22**, 4017.
7. X. H. Huang, I. H. El-Sayed, W. Qian and M. A. El-Sayed, *J. Am. Chem. Soc*., 2006, 128, 2115.
8. J. Chen, D. L.Wang, J. F. Xi, L. Au, A. Siekkinen, A. Warsen, Z. Y. Li, H. Zhang, Y. N. Xia and X. D. Li, *Nano Lett*., 2007, **7**, 1318.
9. W. T. Lu, A. K. Singh, S. A. Khan, D. Senapati, H. T. Yu and P. C. Ray, *J. Am. Chem. Soc*., 2010, **132**, 18103.
10. N. W. S. Kam, M. O'Connell, J. A.Wisdom and H. J. Dai, *Proc. Natl. Acad. Sci. U.S.A*., 2005, **102**, 11600.
11. K. Yang, S. Zhang, G. X. Zhang, X. M. Sun, S. T. Lee and Z. Liu, *Nano Lett*., 2010, **10**, 3318.
12. X. Q. Huang, S. H. Tang, X. L. Mu, Y. Dai, G. X. Chen, Z. Y. Zhou, F. X. Ruan, Z. L. Yang and N. F. Zheng, *Nat. Nanotechnol*., 2011, **6**, 28.
13. M. Zhou, R. Zhang, M. A. Huang, W. Lu, S. L.Song, M. P. Melancon, M. Tian, D. Liang and C. Li, *J. Am. Chem. Soc*., 2010, **132**, 15351.
14. Q. W. Tian, M. H. Tang, Y. G. Sun, R. J. Zou, Z. G. Chen, M. F. Zhu, S. P. Yang, J. L. Wang, J. H. Wang and J. Q. Hu, *Adv. Mater*., 2011, **23**, 3542.
15. C. M. Hessel, V. P. Pattani, M. Rasch, M. G. Panthani, B. Koo, J. W. Tunnell and B. A. Korgel, *Nano Lett*., 2011, **11**, 2560.
16. T. Liu, C. Wang, X. Gu, H. Gong, L. Cheng, X. Z. Shi, L. Z. Feng, B. Q. Sun and Z. Liu, *Adv.*

Mater., 2014, **26**, 3433.

17. L. Cheng, J. J. Liu, X. Gu, H. Gong, X. Z. Shi, T. Liu, C. Wang, X. Y. Wang, G. Liu, H. Y. Xing, W. B. Bu, B. Q. Sun and Z. Liu, *Adv. Mater*., 2014, **26**, 1886.
18. J. Yang, J. Choi, D. Bang, E. Kim, E. K. Lim, H. Park, J. S. Suh, K. Lee, K. H. Yoo, E. K. Kim, Y. M. Huh and S. Haam, *Angew. Chem., Int. Ed*., 2011, **50**, 441.
19. K. Yang, H. Xu, L. Cheng, C. Y. Sun, J. Wang and Z. Liu, *Adv. Mater.*, 2012, **24**, 5586.
20. Y. L. Liu, K. L. Ai, J. H. Liu, M. Deng, Y. Y. He and L. H. Lu, *Adv. Mater*., 2013, **25**, 1353.
21. L. R. Guo, I. Panderi, D. D.Yan, K. Szulak, Y. J. Li, Y. T. Chen, H. Ma, D. B. Niesen, N. Seeram and A. A. Ahmed, *ACS Nano*, 2013, **7**, 8780.
22. L. Cheng, C. Wang, L. Z. Feng, K. Yang and Z. Liu, *Chem. Rev*., 2014, **114**, 10869.
23. B. Li, Q. Wang, R. J. Zou, X. J. Liu, K. B. Xu, W. Y. Li and J. Q. Hu, *Nanoscale*, 2014, **6**, 3274.
24. X. G. Ding, C. H. Liow, M. X. Zhang, R. J. Huang, C. Y. Li, H. Shen, M. Y. Liu, Y. Zou, N. Gao, Z. J. Zhang, Y. G. Li, Q. B. Wang, S. Z. Li and J. Jiang, *J. Am. Chem. Soc*., 2014, **136**, 15684.
25. M. Kumar and C. Persson, *Appl. Phys. Lett*., 2013, **102**, 062109.
26. H. Z. Sun, H. Y. Li, I. Harvey and P. J. Sadler, *J. Biol. Chem*., 1999, **274**, 29094.
27. Y. L. Liu, K. L. Ai and L. H. Lu, *Acc. Chem. Res*., 2012, **45**, 1817.
28. B. Li, K. C. Ye, Y. X. Zhang, J. B. Qin, R. J. Zou, K. B. Xu, X. J. Huang, Z. Y. Xiao, W. J. Zhang, X. W. Lu and J. Q. Hu, *Adv. Mater*. 2015, **27**, 1339.
29. Y. Yang, H. X. Wu, B. Z. Shi, L. L. Guo, Y. J. Zhang, X. An, H. Zhang and S. P. Yang, *Part. Part. Syst. Charact*. 2015, 32, 668.
30. G. Kong, R. D. Braun and M. W. Dewhirst, *Cancer Res*., 2000, **60**, 4440.
31. V. Milani, M. Lorenz, M. Weinkauf, M. Rieken, A. Pastore, M. Dreyling and R. Issels, Int. *J. Hyperther*., 2009, **25**, 262.
32. H. Y. Liu, D. Chen, L. L. Li, T. L. Liu, L. F. Tan, X. L.Wu and F. Q. Tang, *Angew. Chem. Int. Ed*., 2011, **50**, 891.
33. J. Bai, Y. W. Liu and X. E. Jiang, *Biomaterials*, 2014, **35**, 5805.
34. J. B. Yin and J. H. Jia, *CrystEngComm*, 2014, **16**, 2795.

35. H. Otsuka, Y. Nagasaki and K. Kataoka, *Adv. Drug Delivery Rev*., 2003, **55**, 403.

36. W. Eck, G. Craig, A. Sigdel, G. Ritter, L. J. Old, L. Tang, M. F. Brennan, P. J. Allen and M. D. Mason, *ACS Nano*, 2008, **2**, 2263.

37. Z. Liu, J. T. Robinson, X. M. Sun and H. J. Dai, *J. Am. Chem. Soc*., 2008, **130**, 10876.

38. D. E. Owens and N. A. Peppas, *Int. J. Pharm*., 2006, **307**, 93.

39. Q. W. Tian, F. R. Jiang, R. J. Zou, Q. Liu, Z. G. Chen, M. F. Zhu, S. P. Yang, J. L. Wang, J. H. Wang and J. Q. Hu, *ACS Nano*, 2011, **5**, 9761.

40. G. Ku, M. Zhou, S. L. Song, Q. Huang, J. Hazle and C. Li, *ACS Nano*, 2012, **6**, 7489.

41. Y. X. Zhao, H. C. Pan, Y. B. Lou, X. F. Qiu, J. J. Zhu and B. Clemens, *J. Am. Chem. Soc*., 2009, **131**, 4253.

42. D. K. Roper, W. Ahn and M. Hoepfner, *J. Phys. Chem. C*, 2007,**111**, 3636.

43. Q. W. Tian, J. Q. Hu, Y. H. Zhu, R. J. Zou, Z. G. Chen, S. P. Yang, R. W. Li, Q. Q. Su, Y. Han and X. G. Liu, *J. Am. Chem. Soc*., 2013, **135**, 8571.

44. G. S. Song, Q. Wang, Y. Wang, G. Lv, C. Li, R. J. Zou, Z. G. Chen, Z. Y. Qin, K. K. Huo, R. G. Hu and J. Q. Hu, *Adv. Funct. Mater*., 2013, **23**, 4281.

45. J. You, G. D. Zhang and C. Li, *ACS Nano*, 2010, **4**, 1033.

46. X. D. Zhang, J. Chen, Y. Min, G. B. Park, X. Shen, S. S. Song, Y. M. Sun, H. Wang, W. Long, J. P. Xie, K. Gao, L. F. Zhang, S. J. Fan, F. Y. Fan and U. Jeong, *Adv. Funct. Mater*., 2014, **24**, 1718.

47. J. Liu, X. P. Zheng, Liang. Yan, L. J. Zhou, G. Tian, W. Y. Yin, L. M. Wang, Y. Liu, Z. B. Hu, Z. J. Gu, C. Y. Chen and Y. L. Zhao, *ACS Nano*, 2015, **9**, 696.

Graphical Table of Contents